Inelastic scattering of π^+ and π^- mesons from ^{3}He and ^{4}He at energies of 350, 400, and 475 MeV

J. Boswell, G. S. Das, P. C. Gugelot, J. Källne,* J. McCarthy, L. Orphanos, R. C. Minehart, C. Smith, and R. R. Whitney
Institute for Nuclear and Particle Physics, University of Virginia, Charlottesville, Virginia 22901

P. A. M. Gram
Los Alamos National Laboratory, Los Alamos, New Mexico 87545
(Received 21 March 1985)

The momentum distributions of pions inelastically scattered from ^{3}He and ^{4}He were measured for incident energies of 350, 400, and 475 MeV. Pions were detected in a magnetic spectrometer at scattering angles of 60°, 90°, and 120°. The spectra show quasifree scattering from single nucleons along with a substantial component of lower momentum pions. The results are compared to a simple impulse approximation model, which accounts for the principal features of the data, but does not reproduce the low momentum tail even with the inclusion of multiple scattering.

I. INTRODUCTION

Experimental studies of pion-nucleus interactions have included many measurements of pion-nucleus elastic and inelastic scattering, single nucleon knockout by pions, pion charge exchange scattering, and pion absorption (a process which cannot occur on free nucleons). For energies from about 100 to 300 MeV, the region of the Δ resonance, the nonabsorptive reaction cross section[1–12] is dominated by quasifree scattering (QFS), the knockout of a single nucleon by the pion while the rest of the nucleus acts as a spectator. In an inclusive scattering experiment, in which only the scattered particle is detected, the signature of quasifree scattering is a broad peak in the energy spectrum of the scattered particle. The center of the peak is shifted slightly downward from the "free" energy loss, $\Delta E = q^2/2M$ (q is the momentum transfer and M the nucleon mass) by an amount, ϵ, which is primarily due to binding energy of the knocked-out nucleon. The width of the peak is due mainly to the momentum distribution of the struck nucleon, i.e., it is approximately $2qK_F/M$ (K_F is the Fermi momentum).

QFS singles out a one-step process, which can be related to the πN scattering operator in the nuclear medium. At the QFS peak there is little mismatch between energy and momentum transfer, i.e., the scattering is essentially on-shell. Therefore, the maximum of the wave function dominates the reaction process; since this occurs at momenta $q < k_f$, high momentum components will not be important. In an inclusive measurement, summation over the final nuclear states tends to eliminate any dependence on the fine details of the nuclear structure.

The QFS peak is also observed for inclusive electron scattering,[13–16] where it is to be anticipated from the weakness of the electron-nucleon interaction—the chance that an electron will scatter twice in the same nucleus is very small. Pions, on the other hand, interact strongly and the mean free path in the nucleus is smaller than the nucleus. The probability of multiple collisions should be large. Inelastic inclusive scattering of protons, which also interact strongly, in the energy range from 100 to 800 MeV on a variety of nuclei behaves as expected,[17,18] with no pronounced peak observed. The apparently anomalous behavior of pion scattering at energies below 300 MeV is attributed to the high probability for pion absorption. Pions which interact more than once are unlikely to emerge into the inelastic spectrum and obscure the single scattering peak.

To increase our understanding of the energy dependence of QFS for pions we have extended the measurements of the inclusive pion scattering in ^{3}He and ^{4}He to energies above the Δ resonance (350, 400, and 475 MeV). The choice of ^{3}He and ^{4}He was motivated by several considerations. First, their wave functions are well known from electron scattering.[19] Second, the small number of nucleons reduces the contribution of multistep processes and admits the possibility of tractable microscopic calculations. Third, their high density may result in significant changes to the πN scattering operator by the nuclear medium. Moreover, through comparison of the π^+ and π^- QFS cross sections, ^{3}He with two protons and one neutron offers the possibility to study the effect of the isospin dependence of the elementary π-N interaction. The ratio of the total elastic cross sections for π^+p and π^-p, for example, changes from 9.3 at 175 MeV to 1.8 at 500 MeV. The measurement of scattering from ^{4}He checks the relative normalization of the flux monitors for the incident π^+ and π^- beams, since the π^+ and π^- cross sections should be identical.

II. EXPERIMENTAL METHOD

Pions from the P^3 beam line at LAMPF were focused on a target located at the pivot point of the large acceptance spectrometer (LAS).[20] The targets used were ^{3}He, ^{4}He, CH_2, ^{12}C, and ^{27}Al. The CH_2 and ^{12}C targets were used to normalize the observations to the π-p elastic scattering cross section, while the ^{27}Al target was used to determine the background from the aluminum walls in the helium cryostat.

The incident pion flux was measured by a pair of scintillation telescopes designed to detect muons from pion decay in flight.[21] These were placed upstream from the target and set to detect particles emerging on either side of the beam at an angle of 5°. An additional monitor, an ionization chamber, was placed in the beam 5 m downstream from the target. The calibration of the ionization chamber was dependent on the target in the beam, but with a given target the ionization chamber and the π-μ monitors were stable relative to each other to within a few percent. As another test of monitor stability, we kept a running account of the ratio of the raw event rate in the spectrometer to the π-μ monitor rate during each run. This ratio remained constant within statistical accuracy. The calibration was done for each energy and charge of the incident beam by observing scattering from CH_2 and ^{12}C targets, where the ^{12}C data were used for background subtraction.

The target system was a cryostat[19,22] containing liquid ^3He and superfluid ^4He in separate, identical cells. The target cells were mounted one above the other inside the cryostat and were of rectangular cross section, 15 cm wide by 10 cm high, with their thickness varying from 2.5 cm at the edges to 3.75 cm in the middle. The front and back windows were made of 0.094 cm-thick aluminum.

The LAS is a quadrupole-quadrupole-dipole (QQD) system equipped with a scintillator, $S1$, at its entrance and two five-element scintillator hodoscopes, $S2$ and $S3$, at the end. A coincidence between these detectors serves as the event signal. The time difference between $S1$ and $S2$ measures the time of flight of the particle. To measure its trajectory through the spectrometer there are four sets of multiwire proportional chambers, each with an x and a y plane. The first set is located immediately following $S1$ in front of the first quadrupole magnet. The second set is between the second quadrupole magnet and the dipole magnet. The third and fourth sets follow the dipole and are separated by 1 m. Using the trajectory measurements, the momentum of the scattered pions was measured. In a momentum range of $\pm 10\%$ around the central momentum, the resolution was approximately 1.2% (standard deviation). A range of 8° in scattering angle was accepted. At each angle, spectra were measured at three or four settings of the spectrometer's central momentum and combined after unfolding the measured spectrometer acceptance.

III. DATA REDUCTION

The momentum and scattering angle for each trajectory in the spectrometer was determined from a χ^2 minimization procedure to fit the eight measured x-y coordinates to the five starting parameters for the particle, namely x, y, dx/dz, dy/dz, and dp/p at the target. The coordinate z is along the axis of the spectrometer, while x and y are perpendicular to it with x being vertical (in the bend plane of the spectrometer) and y horizontal. The χ^2 distribution from this analysis always gave a sharp peak near $\chi^2=0$. Events for which the χ^2 was more than six times the standard deviation of this peak were discarded. Approximately 90% of the otherwise acceptable events passed this χ^2 test. The observed values of χ^2 imply that each wire plane has a position uncertainty of 0.3 cm, a value consistent with the properties of the wire chambers and multiple scattering in the spectrometer. Most of the events in which the pion decayed to a muon or scattered from pole tips or other apertures should fail the χ^2 test. Another test for the contribution from pion decay and scattering was derived from a study of the momentum spectra of the pions scattered from protons in CH_2. Spectra from CH_2 alone show a peak on a smoothly varying background. When the ^{12}C spectrum is subtracted from the CH_2 spectrum, events generally remain only in the π-p peak region. Thus, either the contamination from decay muons is very small or is confined to a momentum region close to that of the original pions. In all cases less than 10% of the accepted data were outside the momentum peak for π-p scattering, even at the lowest momentum studied.

Several additional cuts were made to reduce the background even further. Cuts were made on the projected target coordinates to define the beam spot on the target. Limits were also placed on the vertical scattering angle, and on the wire chamber coordinates themselves. The various cuts for a typical run are illustrated in Fig. 1.

Protons were eliminated by measuring the time of flight from scintillators $S1$ to $S2$ and $S3$. The electronic time gate of 20 ns for this coincidence eliminated all protons with momenta lower than about 600 MeV/c and a software cut on the scintillation pulse heights removed the rest. Background from the aluminum walls of the target, which was typically 5—10 % of the signal, was subtracted using spectra measured with the aluminum targets.

To calibrate the pion flux monitors, measurements were taken with a CH_2 and a ^{12}C target. After subtracting the carbon background from the CH_2 data, the data in the πp peak were summed. The phase shifts of the Karlsruhe[23] analysis of the world π-N data were used to obtain the cross section for πp scattering. This was combined with our summed data to obtain the incident pion flux, from which the monitors could be calibrated. The same cuts and pion decay corrections used for the π-He analysis were applied to the normalization data. There remain some systematic differences which may contribute to uncertainty in the normalization. First, the momentum spread of pions scattered from protons is large enough for the integrated number to be sensitive to the details of the LAS acceptance. Second, the much stronger dependence of momentum on scattering angle for π-p scattering than for π-He scattering is coupled through second order effects into the LAS acceptance function. Third, the ^{12}C background is large and varying in the region of the π-p peak, so that a difference in the relative angular orientation of the two targets can affect the ^{12}C background subtraction. We estimate that each of these factors could contribute an uncertainty in the normalization of as much as 10%.

The normalized spectra at a given energy and angle for π^+ and π^- scattering were found to be similar for the ^4He and ^{12}C targets. Since ^4He and ^{12}C both have isotopic spin of 0, this is to be expected. However, some discrepancies outside the statistical error were observed. Consequently, we integrated the spectra for ^4He over the

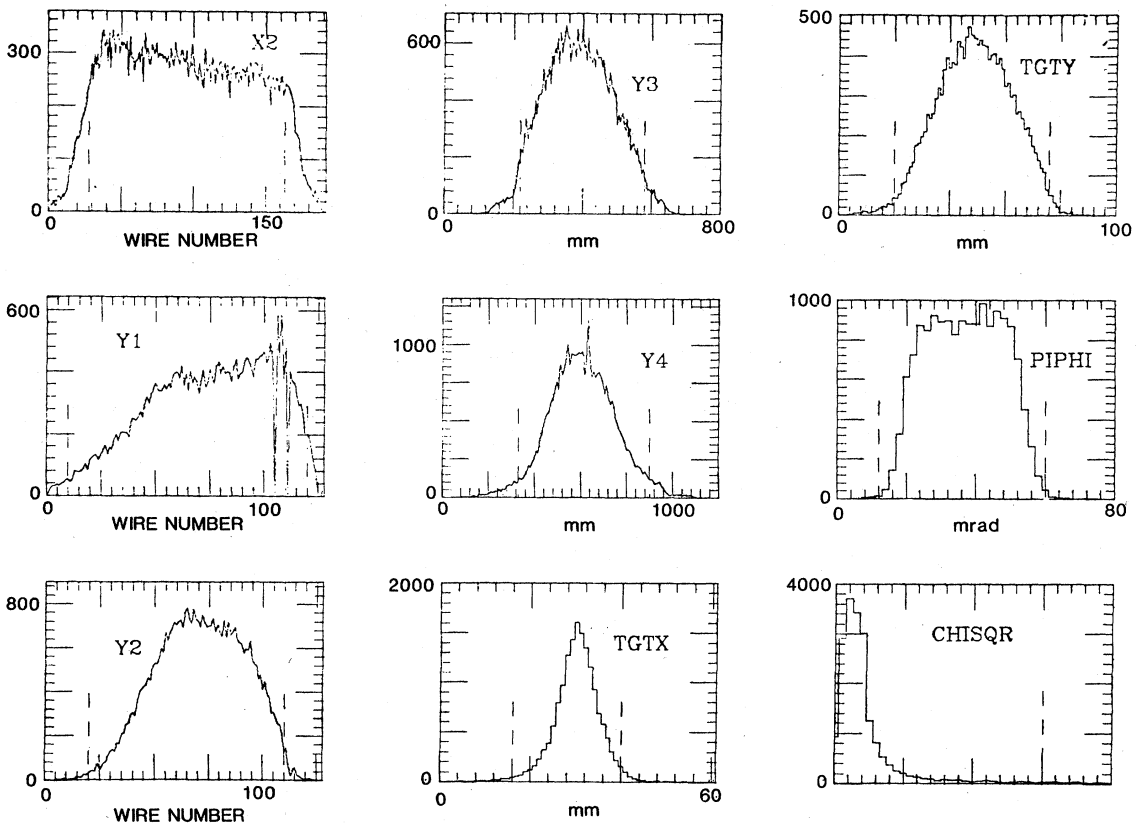

FIG. 1. Histograms of variables for which cuts were made in selecting data used for final analysis. The vertical dashed lines show the cut points. $X2$ is the coordinate in the second wire chamber in the bend plane. $Y1$, $Y2$, $Y3$, and $Y4$ are the coordinates in the four chambers in the horizontal plane. *TGTX* and *TGTY* are projected x and y coordinates at the target, where x is vertical and y is horizontal. *PIPHI* is the pion angle at the entrance to the spectrometer measured in the bend plane. *CHISQR* is the χ^2 value obtained from the fitting routine used to calculate the pion momentum, coordinates, and angles at the target.

region of the expected QFS peak (between the 10% points) and adjusted the normalizations to make the π^+ and π^- sums at a given angle and energy agree. With this normalization the π^+ and π^- spectra for ^{12}C are also in satisfactory agreement. However, our measurements of the π-p cross sections do not then agree within the statistical error with tabulated cross sections. To show the extent of this disagreement, our measured π-p cross sections

TABLE I. Comparison of π-p measured cross sections to cross sections obtained from phase shifts.

		π^+p		π^-p	
T_π (MeV)	θ	(mb/sr) Measured	(mb/sr) Karlsruhe phase shifts	(mb/sr) Measured	(mb/sr) Karlsruhe phase shifts
350	60°	3.2	3.00	0.86	0.96
350	90°	0.63	0.63	0.41	0.39
350	120°	1.2	1.03	0.47	0.40
400	60°	2.70	2.03	0.73	0.90
400	90°	0.31	0.24	0.22	0.26
400	120°		0.44	0.35	0.38
475	60°	1.35	1.24	0.95	0.87
475	90°		0.03	0.24	0.18
475	120°			0.53	0.87

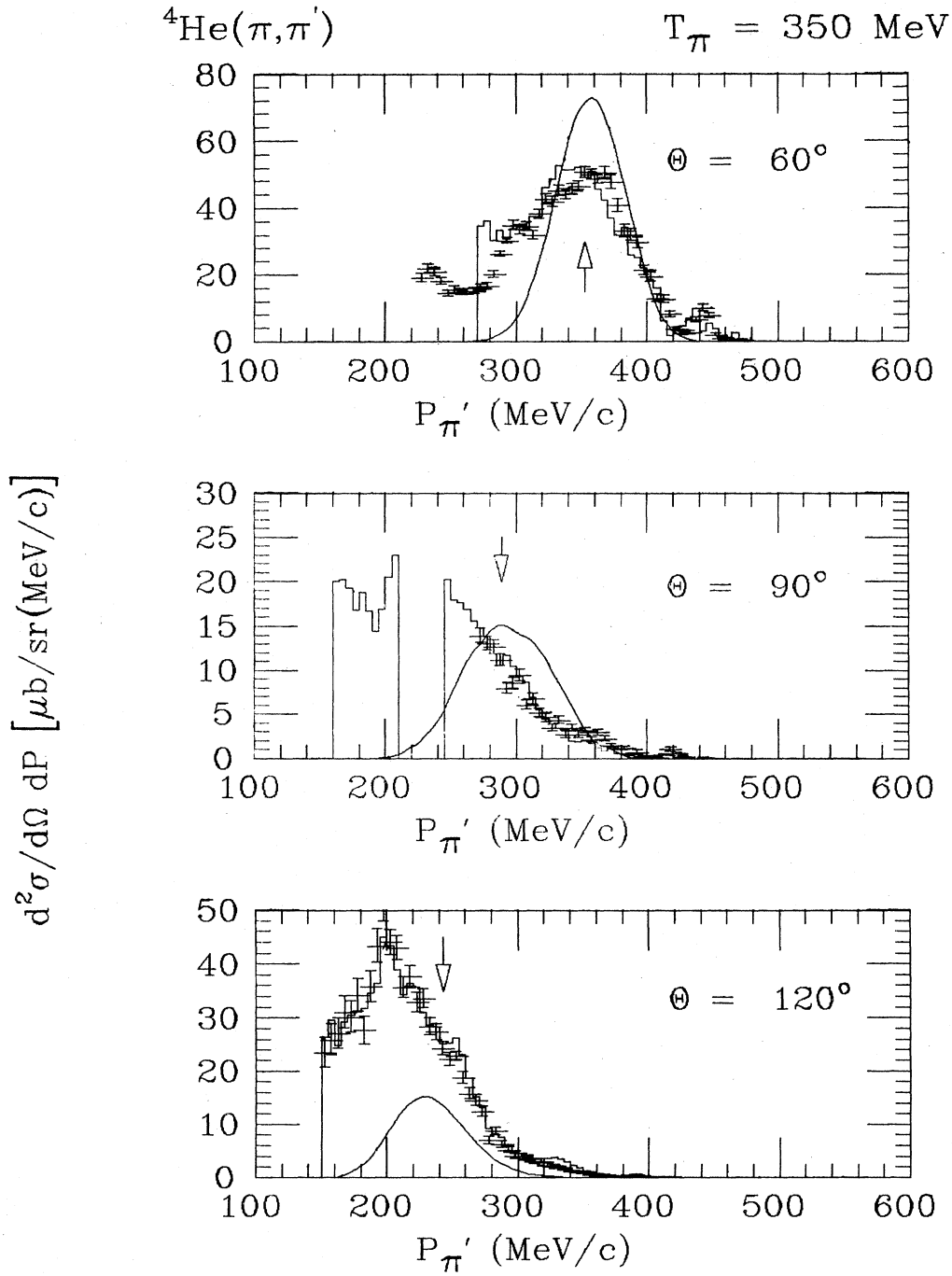

FIG. 2. Momentum distributions for pions with incident energy of 350 MeV scattered from ^{4}He at 60°, 90°, and 120°. The data for π^+ are plotted in histogram form and the data for π^- are plotted as points with error bars. The solid lines are the results of an impulse model calculation allowing only single scattering. The arrows show the momentum for scattering from a stationary free nucleon whose initial effective mass is reduced by a binding correction.

are compared in Table I to those obtained from the Karlsruhe phase shift tabulation.[23] From these discrepancies the uncertainties in the absolute values of the cross sections are estimated to be of the order of 20% at 350 and 475 MeV and 30% at 400 MeV. Systematic errors in the π^+ to π^- ratio are much smaller.

IV. DISCUSSION OF THE RESULTS

The observed spectra are shown in Figs. 2—10. Tabulations of these data are available from the authors. The errors shown include the statistical uncertainties along with an estimate of the effects of uncertainties in the accep-

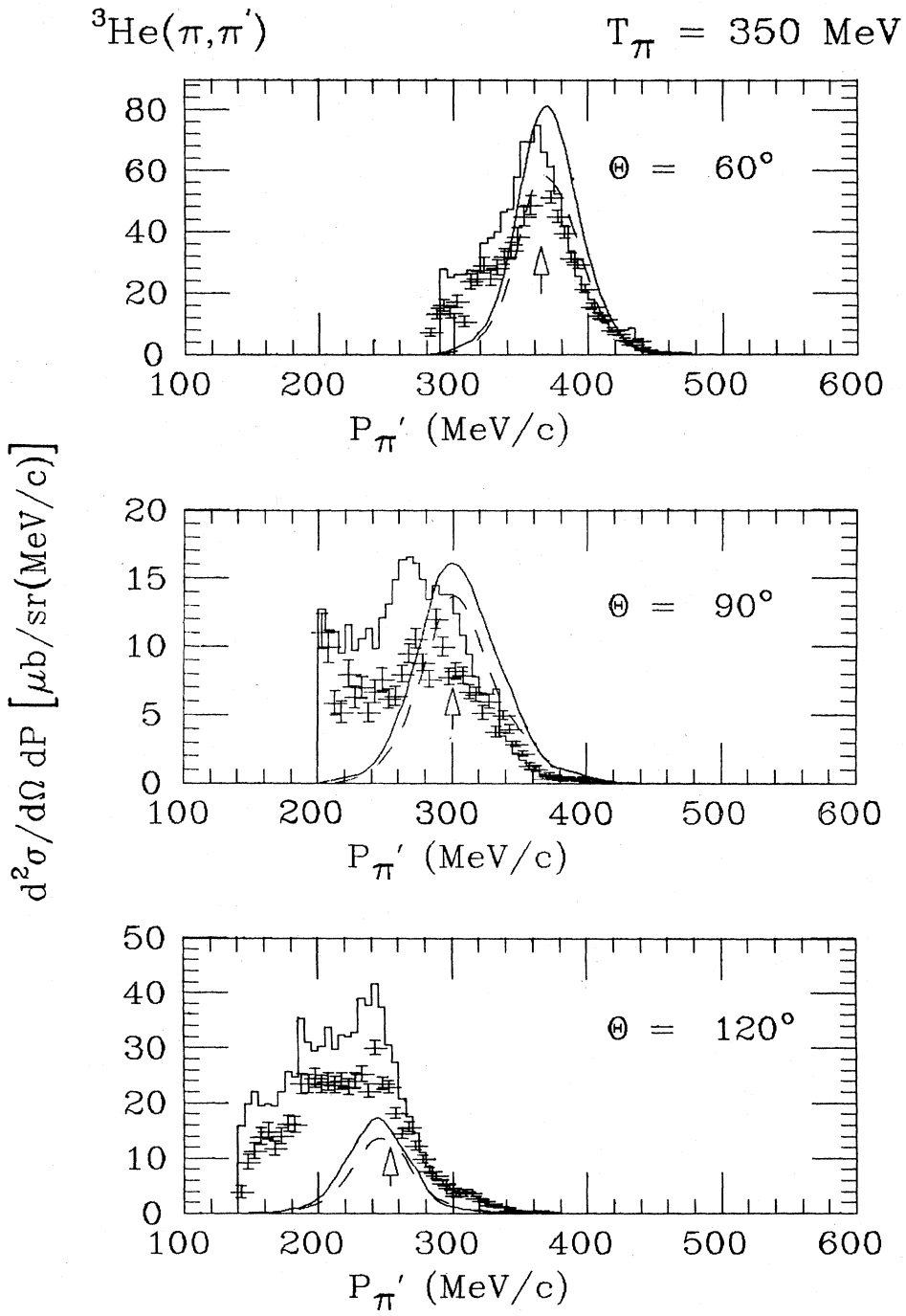

FIG. 3. Momentum distributions for pions with incident energy of 350 MeV scattered from ^{3}He at 60°, 90°, and 120°. The data for π^+ are plotted in histogram form and the data for π^- are plotted as points with error bars. The solid and dashed lines are the results of an impulse model calculation allowing only single scattering for π^+ and π^-, respectively. The arrows show the momentum for scattering from a stationary free nucleon whose initial effective mass is reduced by a binding correction.

tance correction. The arrows in the figures indicate the momentum that would be observed for a pion scattering from a stationary nucleon with an effective initial mass $M^* = M - \epsilon_B$ and a final mass M equal to that of the free nucleon. The correction term ϵ_B was set equal to the average nucleon binding energy. It is clear that the inclusive scattering spectra are not dominated by quasifree scattering, in strong contrast to the situation for pions[1–12]

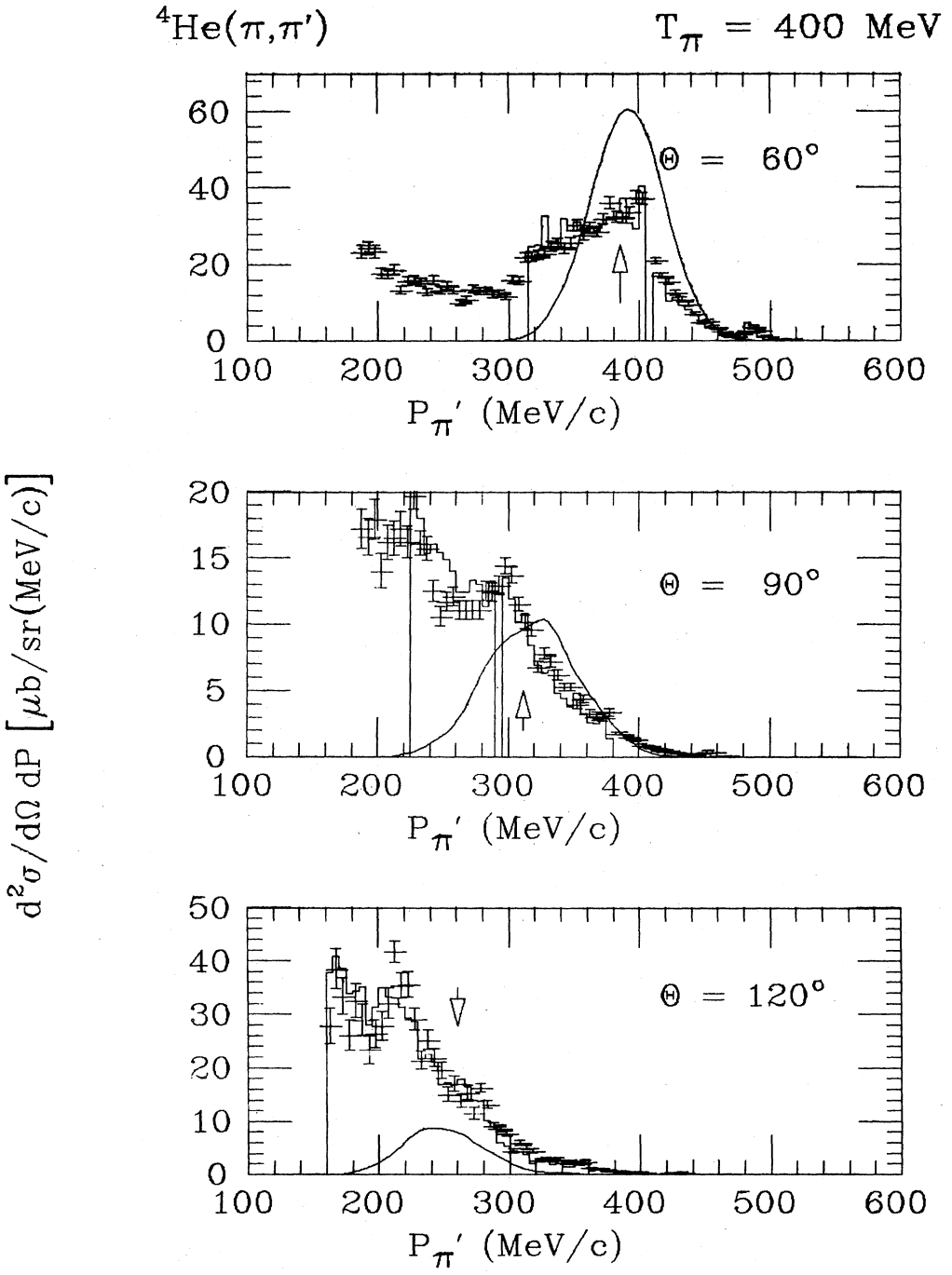

FIG. 4. Same as Fig. 2 but with an incident energy of 400 MeV.

at lower energies. At 90°, where the elementary π-N cross section is lowest, it is difficult to identify any QFS structure in the spectra. At all three energies the spectra for 60° scattering show the QFS peaks most prominently. The peaks in the ^{3}He spectra are narrower and therefore more easily observed than those in the ^{4}He spectra, which is consistent with the relative widths of the nucleon momentum distributions in ^{3}He and ^{4}He.

The ^{3}He and ^{4}He spectra have been compared with a Monte Carlo calculation based on a semiclassical scatter-

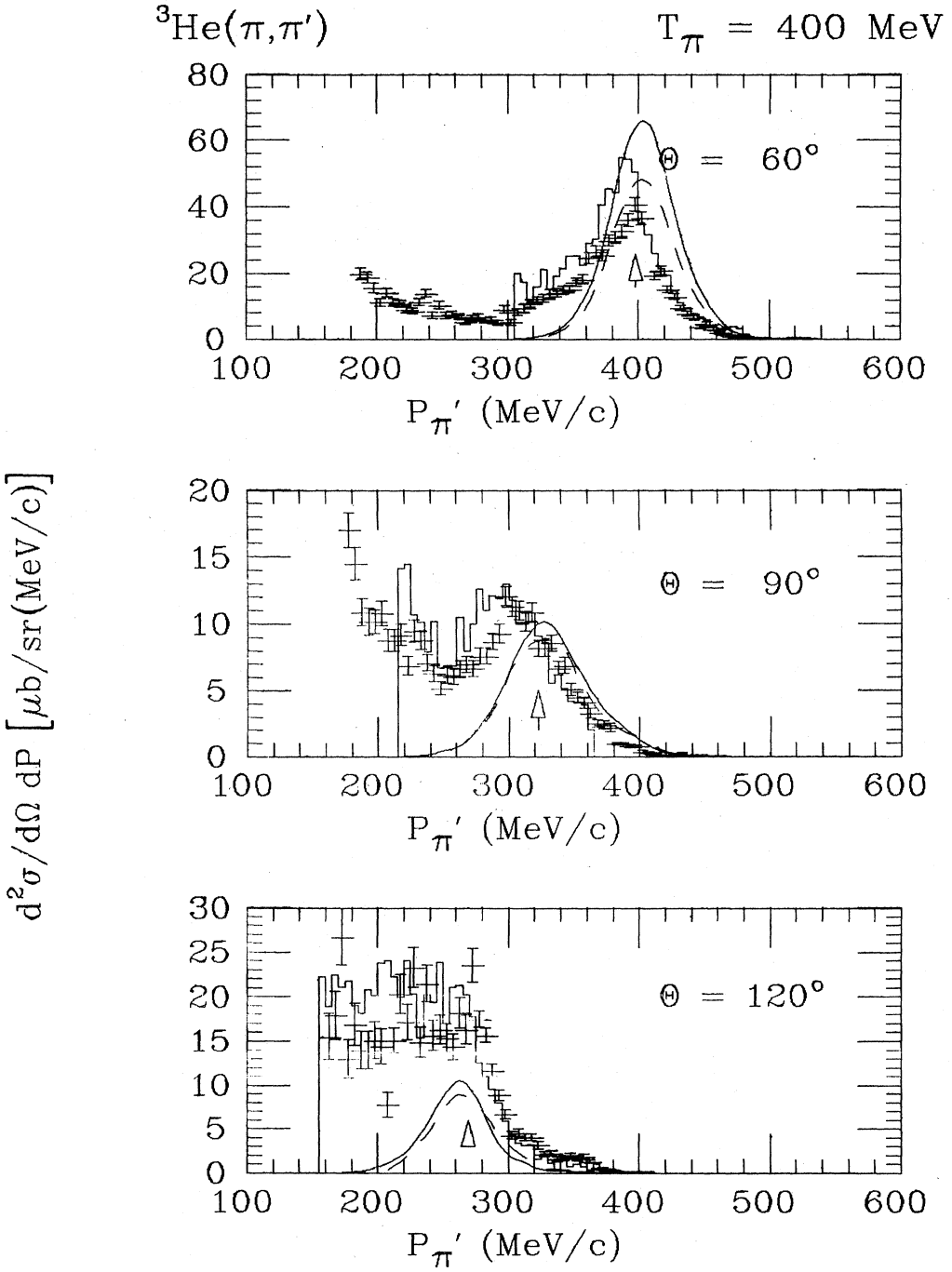

FIG. 5. Same as Fig. 3 but with an incident energy of 400 MeV.

ing model. The pion was assumed to follow a straight line trajectory inside the nucleus before and after the collision with an individual nucleon. Free π-N cross sections, including charge exchange, were used to calculate the probability for successive, uncorrelated scatterings. Nucleon binding was included by using the effective mass M^* for the struck nucleon. To account for the internal momentum of the nucleon, the single particle momentum distribution measured in (e,e'p) scattering by Jans *et al.*[24] was used for ^{3}He, while a Gaussian distribution was used for ^{4}He. The Gaussian was given a width of 70 MeV/c to match the width of the QFS peaks measured at lower energy.[12] Calculations were made with and without multiple scattering. The results for single scattering only are

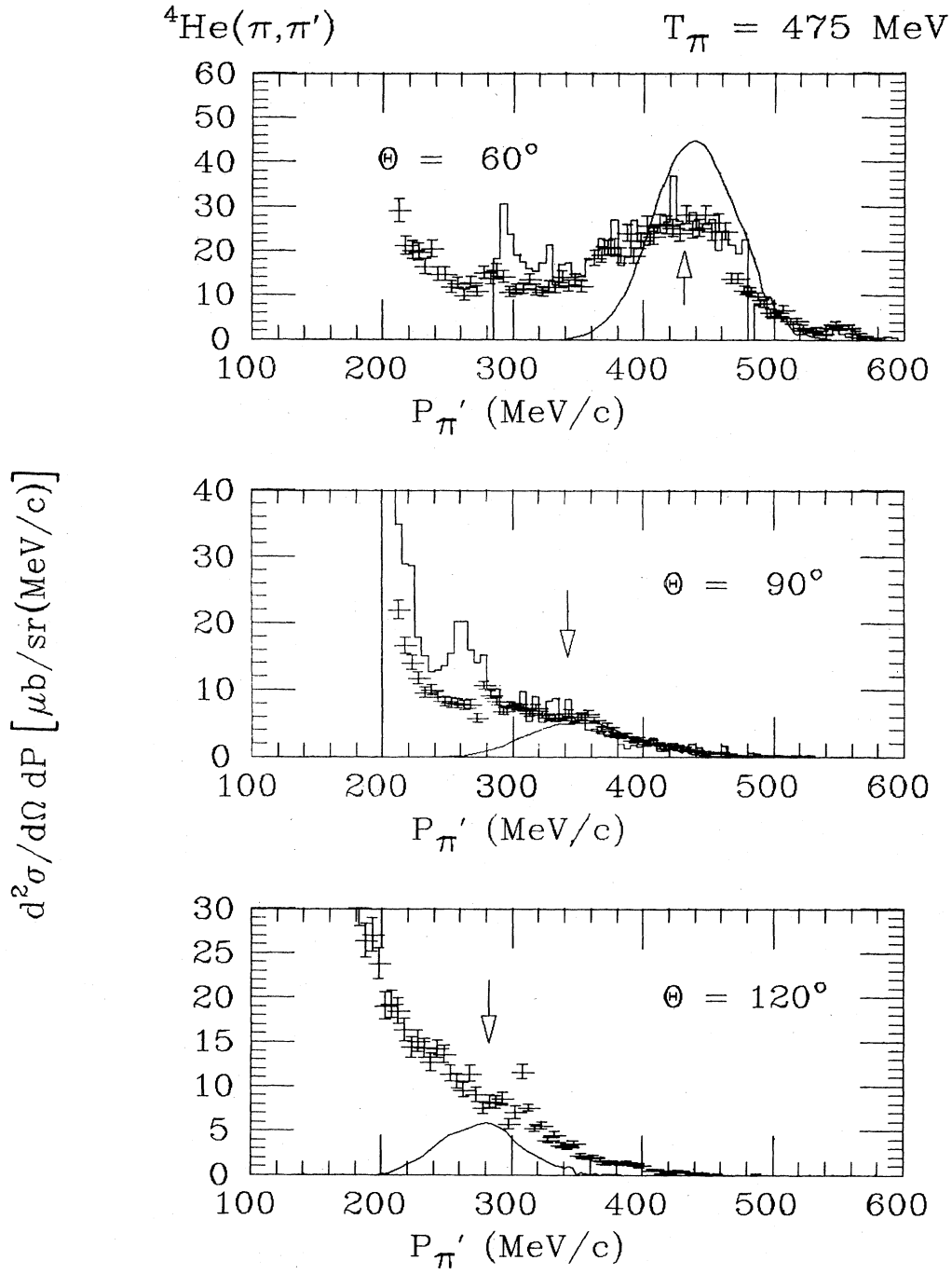

FIG. 6. Same as Fig. 2 but with an incident energy of 475 MeV.

shown in Figs. 2–7.

The calculations for ^{3}He are somewhat more successful at representing the data than are those for ^{4}He. The single scattering calculations with ^{3}He reproduce the shape of the spectra for momenta above the peak, but overestimate the cross section at forward angles, and underestimate it at 120°. At low momenta the single scattering calculation greatly underestimates the measured cross sections. When the pion is allowed to scatter twice in the same nucleus, the agreement at 60° is better, as seen in Fig. 11, but the model still cannot account for the excess low momentum pions. Also, as seen in Fig. 11, the inclusion of double scattering in the model tends to shift the peak towards higher momentum and away from the observed peak position at 90°. This shift is due to the fact that two smaller angle scatterings, for which the cross sec-

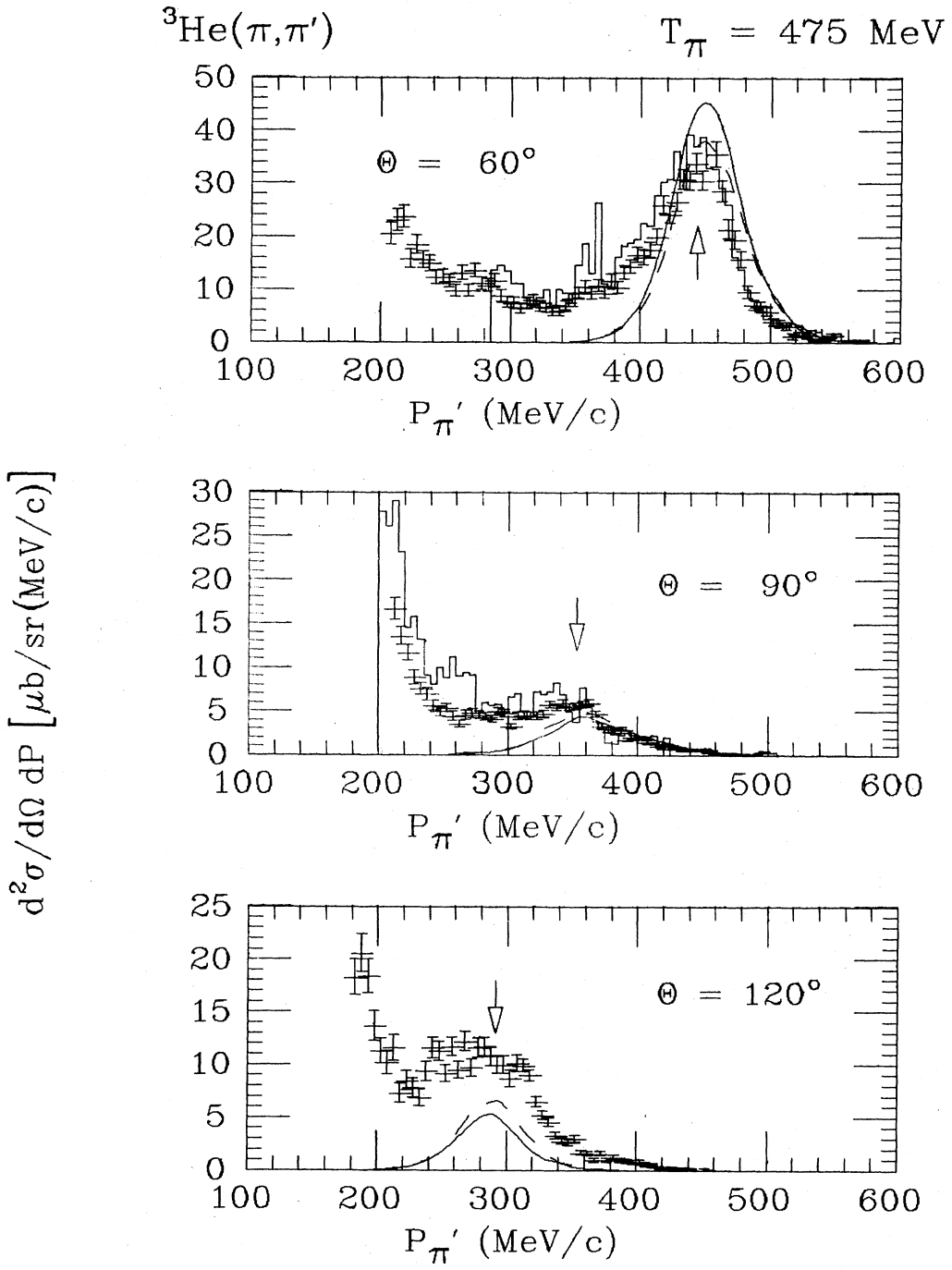

FIG. 7. Same as Fig. 3 but with an incident energy of 475 MeV.

tion is large, can result in a 90° scattering with less momentum loss than that of a single 90° scattering. Although the low momentum component is not reproduced by our model, the double scattering calculation does suggest that multiple scattering can play a significant role at the larger angles where the single scattering cross section is very low. The data for ^{4}He are very difficult to interpret with our model. At momenta just below the elastic scattering the cross section rises at a rate reasonably consistent with the QFS model, but near the momentum where the QFS peak should occur, other processes apparently become important.

In order to make some quantitative statements about the data we have fit the spectra with the function

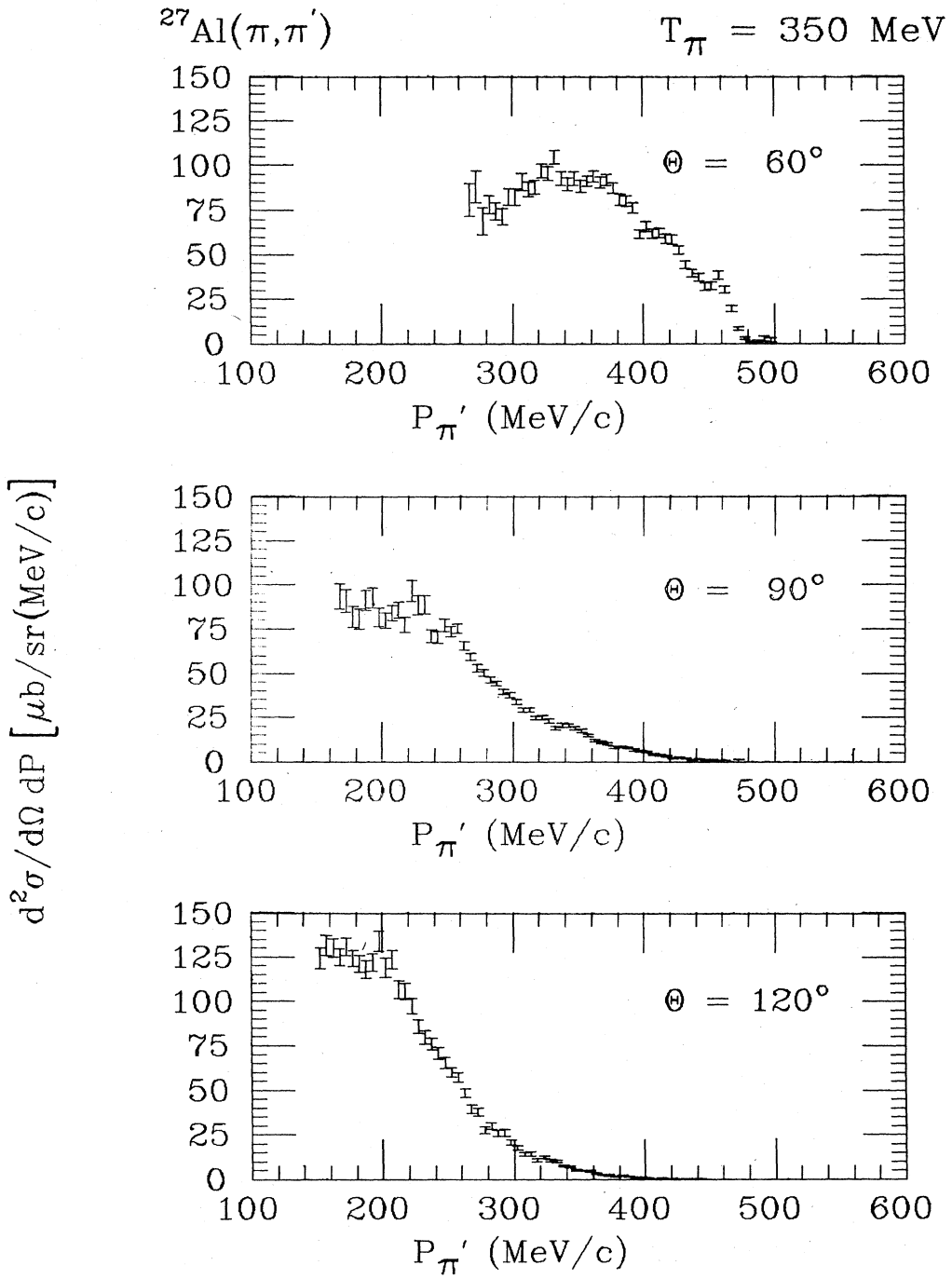

FIG. 8. Momentum distributions for pions with incident energy of 350 MeV scattered from ^{27}Al at 60°, 90°, and 120°. The data for π^+ and π^- were averaged.

$A\exp(-\alpha\cdot p_\pi)+BS(p_\pi)$, where S is the spectral shape obtained from the single scattering approximation model and where the exponential function was chosen to approximate the low energy pion component. It is intended to represent multiple scattering as well as a variety of multibody final states (especially π production) for momenta below the QFS region. For each spectrum, the parameters A and B were varied to get a best fit, and the function BS was integrated to get an estimate of the total QFS component. Some typical results are shown in Fig. 12, and the integrated QFS cross sections are listed in Table II. In several cases, the peak obtained from the single scattering model is clearly at too high a momentum to provide a fit to the high momentum part of the measured spectrum.

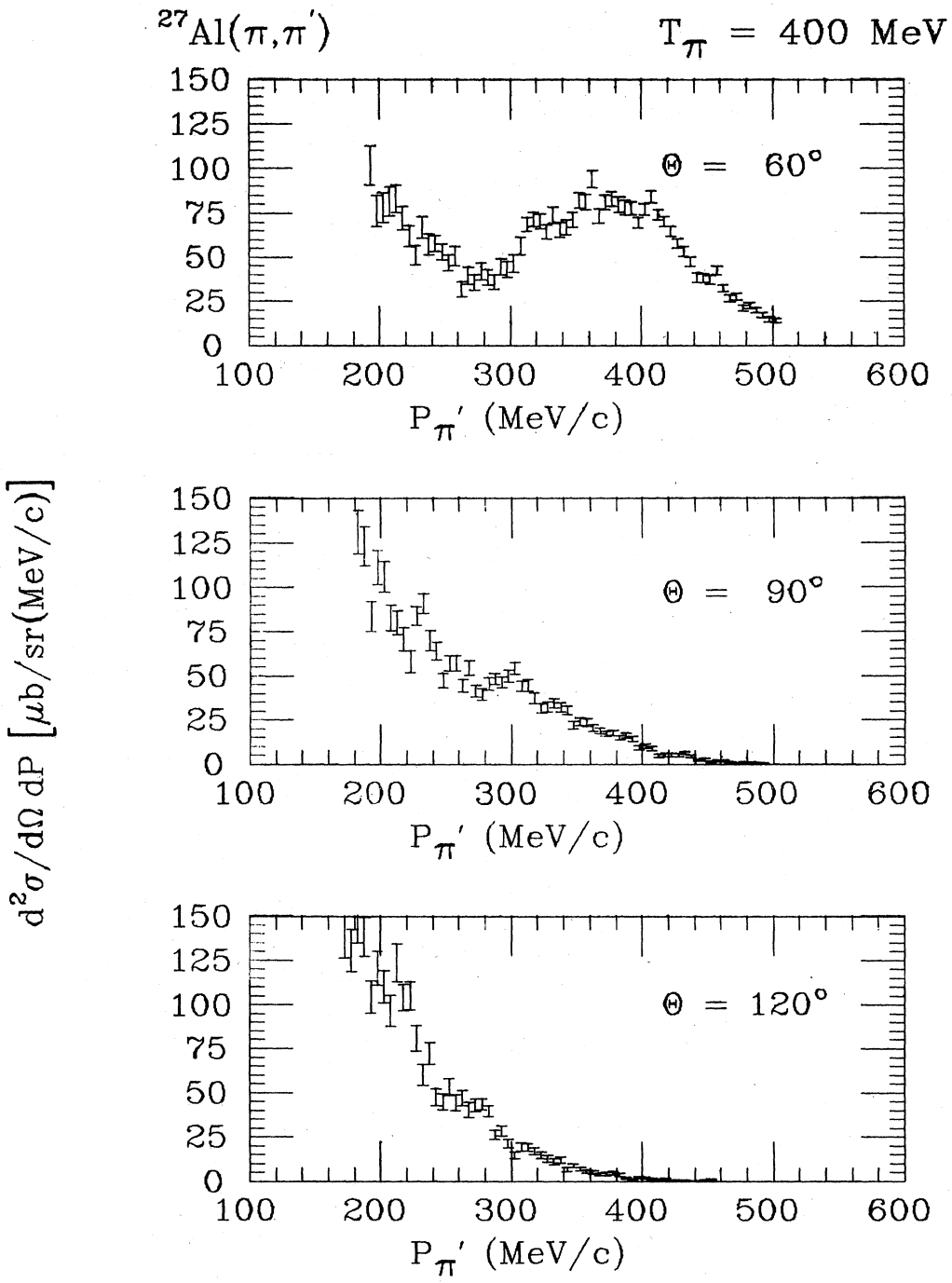

FIG. 9. Same as Fig. 8 but with an incident energy of 400 MeV.

Therefore a second method was also used. The exponential function, as obtained from the fitting procedure, was subtracted from the measured spectrum and the remainder was integrated over the region of the QFS peak. The second set of results is presented in Table III.

The QFS cross sections extracted by these two methods for π^+ and π^- on ^{3}He were compared by taking their ratios, which are listed in Tables II and III. These ratios should reflect the isotopic dependence of the π-N cross section and can be approximated to first order by the simple ratio

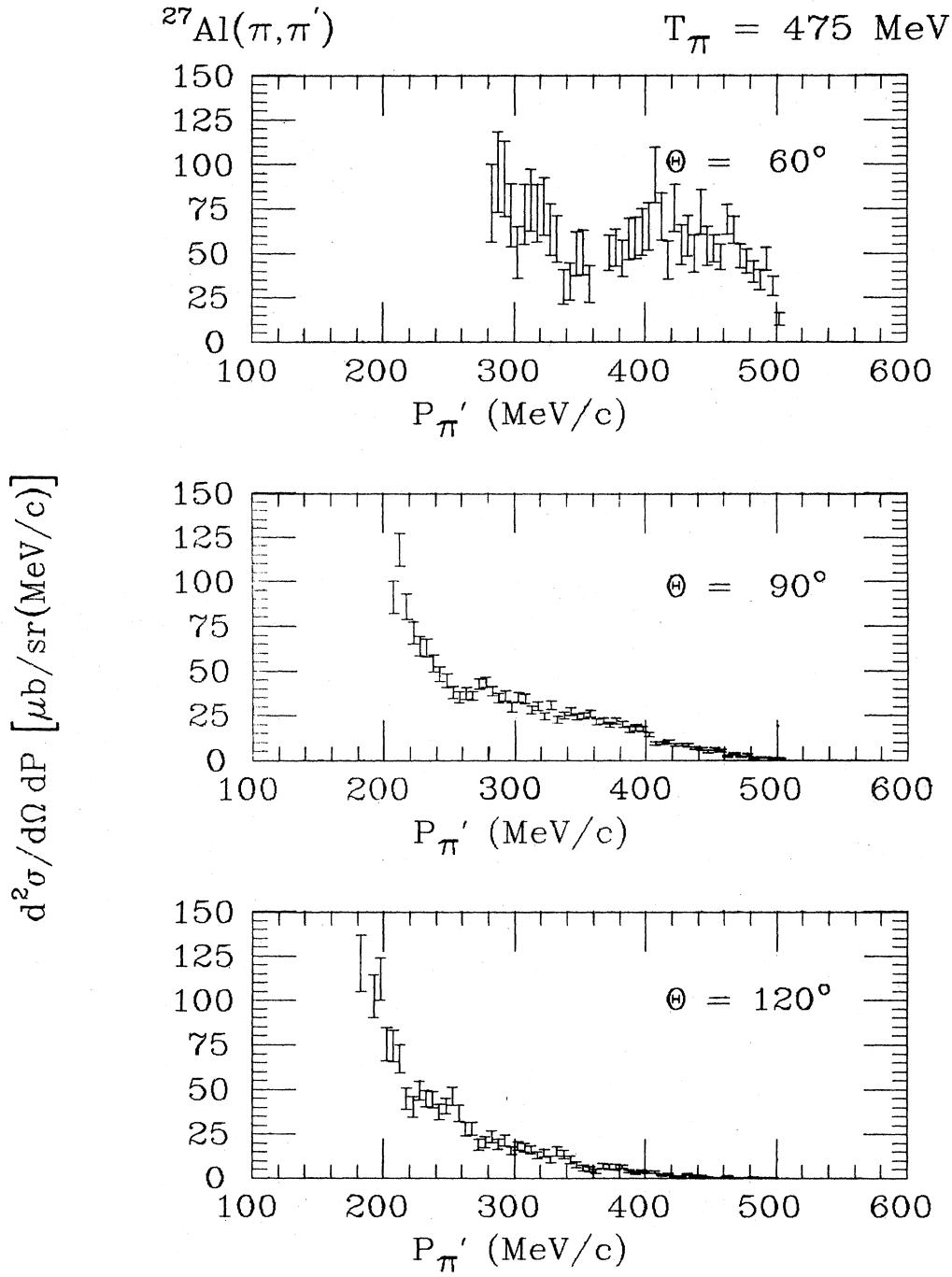

FIG. 10. Same as Fig. 8 but with an incident energy of 475 MeV.

$$\frac{2\frac{d\sigma}{d\Omega}(\pi^+\mathrm{p})+\frac{d\sigma}{d\Omega}(\pi^+\mathrm{n})}{2\frac{d\sigma}{d\Omega}(\pi^-\mathrm{p})+\frac{d\sigma}{d\Omega}(\pi^-\mathrm{n})}, \quad (1)$$

where the differential cross sections are evaluated in the laboratory frame at the scattering angle of interest. The numerical values of this ratio are also listed in Tables II and III for comparison to the integrated QFS cross sections. Although the comparison of the data and the simple ratio is certainly not perfect, the order of magnitude and the trends with energy and angle are in reasonable agreement. The difficulty in extracting true QFS from the data precludes more accurate comparison.

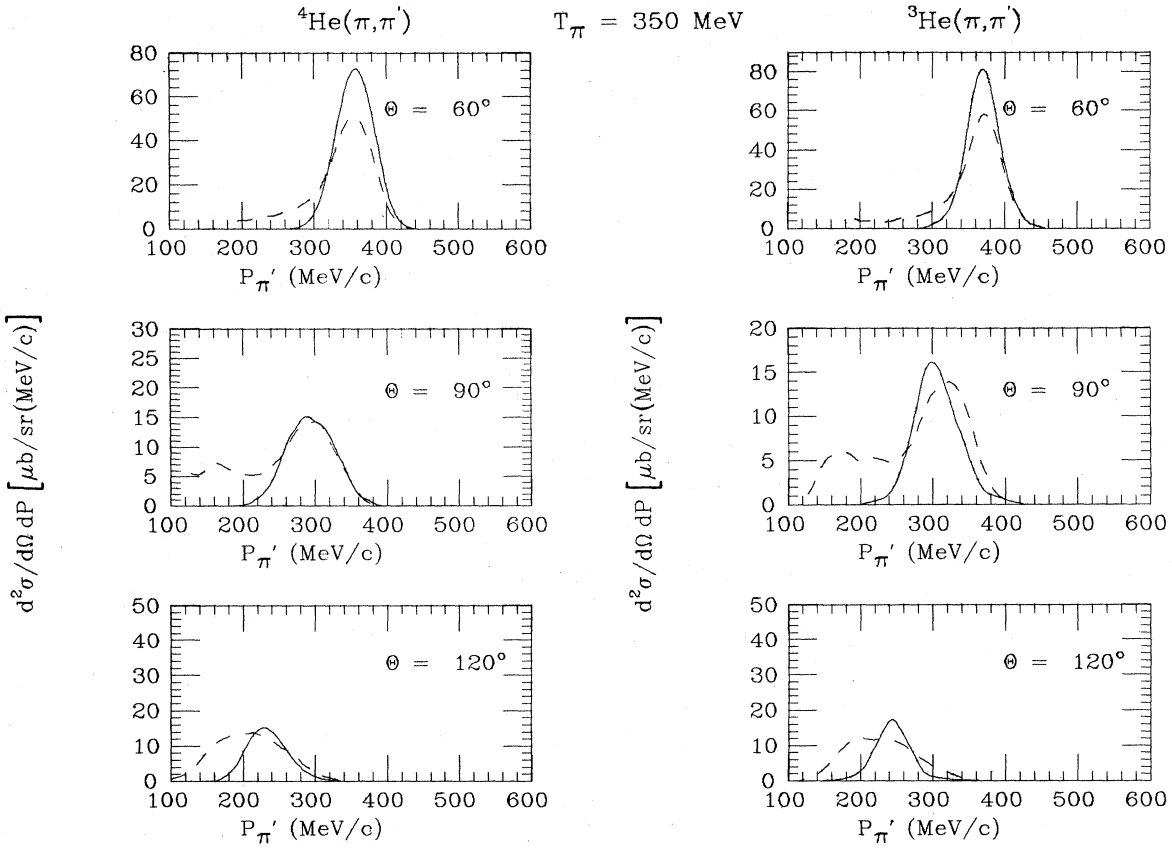

FIG. 11. Comparison of the impulse model calculation allowing double scattering to that allowing only single scattering. The solid line shows the results when the pion was allowed to scatter only once in the nucleus and the dashed line shows the results when two scatterings were allowed.

The cross sections for inclusive pion scattering on ^{4}He measured by Baumgartner *et al.*[8] were found to be fit by a Δ-hole model rather well from 170 to 270 MeV. At 320 MeV the fit to their data was less satisfactory. At that energy the energy spectra for pions scattered into angles around 90° also show a significant contribution from low energy pions. Ingram *et al.*[11] studied pion inelastic scattering in ^{16}O at energies from 114 to 240 MeV and found that at the lower energies the contribution of multiple pion-nucleon collisions was small, while at 240 MeV they accounted for approximately 25% of the cross section. The continuation of this trend to even larger contri-

TABLE II. Cross sections obtained by integrating the calculated single scattering peak fitted along with an exponential background to the data. R is the ratio of the π^+ and π^- cross sections on ^{3}He.

T_π (MeV)	θ	π^+ ^{3}He (mb/sr)	π^- ^{3}He (mb/sr)	π ^{4}He (mb/sr)	R Measured	R Expected
350	60°	3.88	2.99	3.30	1.30	1.41
350	90°	0.69	0.58	0.86	1.19	1.17
350	120°	2.08	1.55	2.10	1.34	1.34
400	60°	2.70	2.29	2.33	1.18	1.30
400	90°	0.67	0.60	0.58	1.12	0.97
400	120°	1.10	1.01	1.36	1.09	1.05
475	60°	2.71	2.38	2.42	1.14	1.12
475	90°	0.30	0.34	0.32	0.88	0.62
475	120°		0.59	0.30		

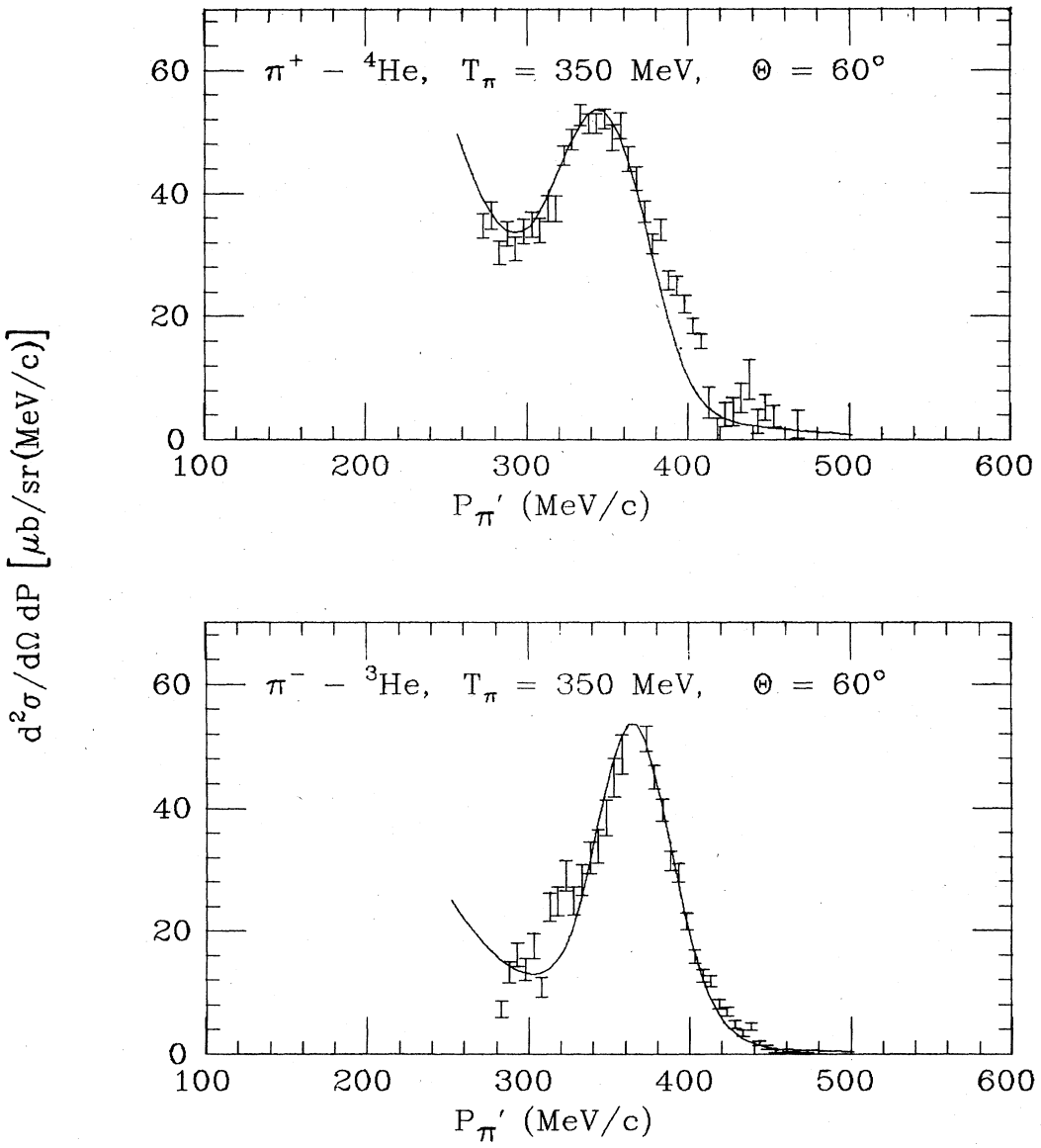

FIG. 12. Examples of the data fit to a combination of an exponential term plus a calculated single scattering peak.

TABLE III. Cross sections obtained by summing over QFS peaks after subtracting an exponential background function. R is the ratio of the π^+ and π^- cross sections on ^{3}He.

T_π (MeV)	θ	$\pi^+ {}^3$He (mb/sr)	$\pi^- {}^3$He (mb/sr)	$\pi {}^4$He (mb/sr)	R Measured	R Expected
350	60°	4.00	2.54	3.47	1.58	1.41
350	90°	0.75	0.55	0.60	1.36	1.17
350	120°	2.40	1.86	1.83	1.29	1.34
400	60°	2.84	2.39	2.49	1.19	1.30
400	90°	0.45	0.67	0.49	0.67	0.97
400	120°	1.22	1.20	1.40	1.02	1.05
475	60°	2.93	2.57	2.70	1.14	1.12
475	90°	0.27	0.35	0.39	0.77	0.62
475	120°		0.58	0.27		

butions from multiple collisions may explain the observations reported here.

There are several reasons to expect larger contributions from multiple scattering at these energies. As discussed by Ingram *et al.*,[11] the following factors tend to reduce the contribution of multiple scattering at energies in the region of the 3-3 resonance:

(1) Pauli blocking limits the scattering of a pion which has already lost a substantial fraction of its energy in a first scattering.

(2) The probability of pion absorption increases with the number of π-N interactions within the nucleus. This tends to remove strength from the multiple scattering process.

(3) At the resonance, the first scattering occurs at an energy for which the cross section is relatively large, while the second occurs at an energy for which the cross section is relatively small.

For energies above the resonance these effects are all less important:

(1) After a first scattering the pion still has too much energy for Pauli blocking to be important.

(2) The cross section for pion absorption becomes relatively less important as the energy is increased above the resonance.

(3) The first scattering occurs at an energy for which the relative π-N interaction tends to be smaller than the cross section at the energy of a second scattering.

Thus, the effects which remove strength from the multiple scattering process for lower energy pions are less important at energies above the resonance, and our observation of a large low energy component in the spectrum of scattered pions may be explicable in terms of multiple scattering. The failure of our simple classical scattering model with multiple scattering included then remains to be explained.

V. CONCLUSIONS

We have measured the inelastic, inclusive spectra of pions scattered from ^{3}He and ^{4}He at energies of 350, 400, and 475 MeV/c. In contrast to the situation for lower energy pions, the cross sections are not dominated by the QFS process. For momenta corresponding to the high energy side of the QFS peak, the magnitude of the cross section is, however, roughly in agreement with an impulse approximation model. A substantial contribution from low energy pions tends to obscure the QFS peak, particularly at large angles. A semiclassical impulse approximation model incorporating multiple scattering is unable to account for this component.

Additional measurements with higher statistical precision and extending to lower values of the momentum of the scattered pion are needed to obtain an accurate value of the total inelastic cross section and the ratio of the QFS to the total cross section. Measurements of exclusive processes in a coincidence experiment are needed to resolve the single scattering part of the cross section and to determine the source of the low momentum component in the inclusive scattering.

ACKNOWLEDGMENTS

This work was supported in part by the U.S. Dept of Energy. We would like to thank the LAMPF staff for their assistance in mounting and operating the LAS spectrometer and the helium cryostat.

---

*Present address: JET, Abingdon, OX14 3EA, England.

[1]L. W. Swenson, T. Sharma, K. Krane, P. Varghese, D. K. McDaniels, H. A. Thiessen, Noby Tanaka, M. Greenfield, and C. F. Moore, Phys. Rev. Lett. **40**, 10 (1978).

[2]J. H. Hoftiezer, S. D. Baker, J. M. Clement, W. H. Dragoset, I. M. Duck, R. D. Felder, D. M. Judd, G. S. Mutchler, G. P. Pepin, G. C. Phillips, E. A. Umland, J. C. Allred, E. V. Hungerford III, B. W. Mayes, L. S. Pinsky, T. M. Williams, M. Furic, and W. von Witsch, Phys. Rev. C **23**, 407 (1981).

[3]D. Ashery, R. J. Holt, H. E. Jackson, J. P. Schiffer, H. R. Specht, K. E. Stephenson, R. D. McKeown, J. Ungar, R. E. Segel, and P. Zupranski, Phys. Rev. Lett. **47**, 895 (1981).

[4]D. Ashery, I. Navon, G. Azuelos, H. K. Walter, H. J. Pfeiffer, and F. W. Schlepütz, Phys. Rev. C **23**, 2173 (1981).

[5]J. Källne and R. R. Whitney, Phys. Lett. **107B**, 23 (1981).

[6]E. Piasetzky, A. Altman, J. Lichtenstadt, A. I. Yavin, D. Ashery, W. Bertl, L. Felawka, H. K. Walter, F. W. Schlepütz, R. J. Powers, R. G. Winter, and J. v.d. Pluym, Phys. Lett. **114B**, 414 (1982).

[7]M. Baumgartner, H. P. Gubler, G. R. Plattner, W. D. Ramsay, H. W. Roser, I. Sick, P. Zupranski, J. P. Egger, and M. Thies, Phys. Lett. **112B**, 35 (1982).

[8]M. Baumgartner, H. P. Gubler, G. R. Plattner, W. D. Ramsay, H. W. Roser, I. Sick, P. Zupranski, J. P. Egger, and M. Thies, Nucl. Phys. **A399**, 451 (1983).

[9]M. D. Cooper, H. W. Baer, J. D. Bowman, F. H. Cverna, R. H. Heffner, C. M. Hoffman, N. S. P. King, J. Piffaretti, J. Alster, A. Doron, S. Gilad, M. A. Moinester, P. R. Bevington, and E. Winkleman, Phys. Rev. C **25**, 438 (1982).

[10]S. M. Levenson, D. F. Geesaman, E. P. Colton, R. J. Holt, H. E. Jackson, J. P. Schiffer, J. R. Specht, K. E. Stephenson, B. Zeidman, R. E. Segel, P. A. M. Gram, and C. A. Goulding, Phys. Rev. C **28**, 326 (1983).

[11]C. H. Q. Ingram, P. A. M. Gram, J. Jansen, R. E. Mischke, J. Zichy, J. Bolger, E. T. Boschitz, G. Probstle, and J. Arvieux, Phys. Rev. C **27**, 1578 (1983).

[12]R. R. Whitney, J. Källne, J. S. McCarthy, R. C. Minehart, R. L. Boudrie, J. F. Davis, J. B. McClelland, and A. Stetz, Nucl. Phys. **A408**, 417 (1983).

[13]J. S. McCarthy, I. Sick, R. R. Whitney, and M. R. Yearian, Phys. Rev. C **13**, 712 (1976).

[14]A. E. L. Dieperink, T. de Forest, I. Sick, and R. A. Branden-

burg, Phys. Lett. **63B**, 261 (1976).
[15]G. Kobschall, E. Fein, C. Otterman, K. Maurer, K. Rohrich, Ch. Schmitt, and V. H. Walther, Nucl. Phys. **A412**, 294 (1983).
[16]D. Day, J. S. McCarthy, I. Sick, R. G. Arnold, B. T. Chertok, S. Rock, Z. M. Szalata, F. Martin, B. A. Mecking, and G. Tamas, Phys. Rev. Lett. **43**, 1143 (1979).
[17]T. Chen, R. E. Segel, P. T. Debevec, John Wiggins, P. P. Singh, and J. V. Maher, Phys. Lett. **103B**, 192 (1981).
[18]R. E. Segel, T. Chen, L. L. Rutledge, Jr., J. V. Maher, John Wiggins, P. P. Singh, and P. T. Debevec, Phys. Rev. C **26**, 2424 (1982).
[19]J. S. McCarthy, I. Sick, and R. R. Whitney, Phys. Rev. C **15**, 1396 (1977).
[20]E. Colton, Nucl. Instrum. Methods **178**, 95 (1980).
[21]E. A. Wadlinger, Nucl. Instrum. Methods **134**, 243 (1976).
[22]L. Orphanos, J. McCarthy, R. C. Minehart, P. A. M. Gram, B. Hoistad, C. F. Perdrisat, and J. Källne, Phys. Rev. C **26**, 2111 (1982).
[23]G. Höhler, F. Kaiser, R. Koch, and E. Pietarinen, Handbook of Pion-Nucleon Scattering, Fachinformationszentrum, Karlsruhe Report 12-1, 1979.
[24]E. Jans, P. Barreau, M. Bernheim, J. M. Finn, J. Morgenstern, J. Mougey, D. Tarnowski, S. Turch-Chieze, S. Frullani, F. Garibaldi, G. P. Capitani, E. De Sanctis, M. K. Brussel, and I. Sick, Phys. Rev. Lett. **49**, 974 (1982).